Grain Boundary Energy and Grain Growth in Highly-Textured Al Films and Foils: Experiment and Simulation

K. Barmak[1, a], W. E. Archibald[2, b], J. Kim[3, c], C.-S. Kim[4, d], A. D. Rollett[5, e], G. S. Rohrer[6, f], S. Ta'asan[7, g], D. Kinderlehrer[8,h]

[1-5]Department of Materials Science and Engineering, Carnegie Mellon University, Pittsburgh, Pennsylvania 15213, USA

[6,7]Department of Mathematical Sciences, Carnegie Mellon University, Pittsburgh, Pennsylvania 15213, USA

[a]katayun@andrew.cmu.edu, [b]wea@andrew.cmu.edu, [c]jihwan@andrew.cmu.edu, [d]changsoo@andrew.cmu.edu, [e]rollett@andrew.cmu.edu, [f]gr20@andrew.cmu.edu, [g]shlomo@andrew.cmu.edu, [h]davidk@andrew.cmu.edu

Keywords: Grain boundary energy, grain growth, thin films, aluminum.

Abstract. Relative grain boundary energy as a function of misorientation angle was measured in a cube-oriented, 120 μm-thick Al foil and in a <111> fiber-textured, 1.7 μm-thick Al film using a multiscale analysis of the grain boundary dihedral angles. For the Al foil, the energies of low-angle boundaries increased with misorientation angle, in good agreement with the Read-Shockley model. For the Al film, two energy minima were observed for high-angle boundaries. Grain growth was studied in 25 and 100 nm-thick films that were annealed at 400 °C for a series of times in the range of 0.5 to 10 h. For the 100 nm-thick film, grains approximately doubled their size (equivalent circular diameter) before grain growth stagnated. The steady-state distributions of reduced grain area for two-dimensional, Monte Carlo Potts and partial differential equation based simulations showed excellent agreement with each other, even when anisotropic boundary energies were used. However, the simulated distributions had fewer small grains than the experimental distributions.

Introduction

In order for computer simulations of grain growth to ultimately predict the behavior of real materials, they will have to include realistic grain boundary properties such as the anisotropy in the grain boundary energy. In addition, it will be necessary to validate the results of grain growth simulations against those of experiments. Toward this end, we have measured the relative grain boundary energy as a function of misorientation angle in a cube-textured, 120 μm-thick foil annealed at 550 °C and in a strongly <111> fiber-textured, 1.7 μm-thick film annealed at 450 °C. Nearly 300 triple junctions were characterized in the Al foil and more than 7000 triple junctions in the Al film. Grain growth was examined in <111> fiber-textured, 25 and 100 nm-thick films of Al annealed 0.5-10 h at 400 °C using transmission electron microscopy. The experimental grain structures were compared with those obtained in two-dimensional (2D) simulations of grain growth that used both the Monte Carlo Potts (MC) model and a partial differential equation (PDE) model that tracked the curvature-driven evolution of the grain boundary network, with the Herring condition enforced at each triple junction.

Experiment

A 120 μm thick foil of 99.98 % pure Al was annealed in Ar-4%H_2 at 550 °C for 9 h to obtain a columnar grain structure with a strong cube, i.e., {001}<100> texture.[1] The sample was air-cooled after annealing and electropolished. The Al films, 25 nm, 100 nm, and 1.7 μm thick, were deposited in an ultrahigh vacuum sputtering system. The substrates were 75 mm diameter oxidized silicon (100) wafers. The oxide thickness was 100 nm. The target purity was 99.99%. The

films were annealed in Ar-4%H_2 to allow the grains to grow and a strong <111> fiber-texture to develop. The 25 nm-thick Al film was annealed at 400 °C for 2 h. The 100 nm-thick film was annealed at 400 °C for 0.5, 1, 2, 4, and 10 h. The 1.7 μm-thick film was annealed at 450 °C for 5h.

For the cube-textured Al foil and the <111> fiber-textured 1.7 μm-thick Al film, electron back scatter diffraction patterns and orientation image maps were obtained using a Philips XL-40 field emission gun scanning electron microscope/orientation imaging microscope (OIM). The scans were performed at 15 kV with the sample tilted at 60 or 70°. The step sizes for the examination of the Al foil and the Al film were 2 μm, and 0.15 (or 0.125) μm, respectively. Grain orientations and misorientations were obtained using the TSL software on the OIM. The dihedral angles at grain boundary triple junctions, i.e., the angles between each pair of boundaries meeting at the triple point, for the Al foil sample were obtained from skeletonized boundary traces of the orientation image maps using either the Linefollow code developed by Mahadevan [1] or a similar code.

The strong cube texture ({001}<100>) of the Al foil and the equally strong <111> fiber-texture of the thin Al film allowed us to determine the relative energies for specific subsets of the full range of grain boundary types. However, for the case of the thin film sample, the larger number of triple junctions allowed a more detailed analysis to be performed. Relative grain boundary energies as a function of misorientation angle were obtained using the technique previously used by Yang et al. [2] to determine boundary energies in Al foils similar to those studied here. In this technique, triple junctions are assumed to be at equilibrium and to obey the Herring equation of tangential and normal (torque) force balance.[3] For simplicity, it is further assumed that the grain boundary energy is independent of boundary orientation, i.e., the torque term is taken to be zero. Each pair of boundaries then obeys equations of the form $\sigma_1 \sin\chi_2 - \sigma_2 \sin\chi_1 = 0$, known as Young's relations, where σ is the energy, χ is the dihedral angle and the subscripts on the energy denote the boundary type. The resultant system of linear equations for all the triple junctions in the dataset is solved using a statistical multiscale method, described in detail elsewhere.[4-7] For the cube-textured Al foil, the number of triple junctions analyzed was 297. For the <111> fiber-textured, 1.7 μm-thick Al film, triple junctions that had one or more abutting grains with a misorientation angle of greater than 10° between the <111> axis of the grain and the normal to the film sample were eliminated from the set. This reduced the number of triple junctions analyzed from 8694 to 7367. The grain structure of the film was assumed to be fully columnar, and the grain boundaries were all assumed to be <111> tilt boundaries. Observations of samples in cross section showed the assumption of a columnar grain structure to be reasonable.

Film texture was characterized for the as-deposited and the 10 h-annealed 100 nm thick-Al samples by measuring the {111} and {200} pole figures in a Philips X'Pert System. Film grain structure for the 25 and 100 nm-thick Al samples was characterized in the transmission electron microscope. The electron transparent samples were obtained by chemically back-etching the silicon and stopping in the oxide layer.[8] The samples were examined in a Philips EM420 microscope operating at 120 kV. The grain boundaries were traced from photographic prints onto transparencies. The black-on-clear tracings of the boundaries were digitally scanned, and the grain area and size, the latter defined as the diameter of a circle of equal area to the grain of interest, was obtained using Scion image in a manner similar to our previous work.[8,9] The dihedral angles were obtained using the Linefollow code mentioned above.[1] Additional details can be found elsewhere.[10]

For grain growth simulations both the Monte Carlo Potts (MC) model and a boundary tracking model termed the partial differential equation (PDE) model were used.[11-14] The PDE simulations portray the evolution of a network of two-dimensional curves governed by the Mullins Equation of curvature driven growth. The Herring Condition of force balance is imposed at each triple junction. For simplicity, the anisotropic energy used here had the form $\sigma = 1 + 0.12\sin^2\theta$, where θ is the misorientation angle. A typical computation began with 25,000 grains and ran until

about 8000 grains remained. Self-similarity of the relative area histograms occurred approximately one-half to two-thirds through the process Additional details can be found elsewhere.[10]

Results and Discussion

The inverse pole figure map, or orientation image map, of the 120 μm-thick Al foil is given in Fig. 1, which because of the strong cube texture ({001}<100>) present in the foil, shows a strong preference for {001} planes at the surface. Grain boundary energies as a function of misorientation for this sample are given in Fig. 2. The energies show good agreement with the results of Yang et al.[2] However, since the variation in energy with misorientation yields relative energies only, the results presented here were multiplied by a constant chosen so as to maximize the agreement in the low angle range where the two datasets overlapped. Figure 2 further shows that for low-angle boundaries, the boundary energy has a reasonable fit to the Read-Shockley dislocation model, namely $E = E_o\theta(A - \ln\theta)$, where E is the boundary energy, E_o is a function of the elastic properties of the material, θ is the misorientation angle across the grain boundary, and A is a constant that depends on the dislocation core energy.[15] For high-angle boundaries, the variation in boundary energy with misorientation is not large (Fig. 2), in agreement with Yang [16] and others [17,18]. The only exception to this statement is for coherent twin boundaries (60° about <111> in pure twist configuration) and ∑11 boundaries with a (113) normal (i.e., a symmetric tilt configuration). Neither of these special boundary types is distinguishable in this (relatively small) dataset, nor are they likely to occur very often in a sample like this which is dominated by 001 tilt boundaries.

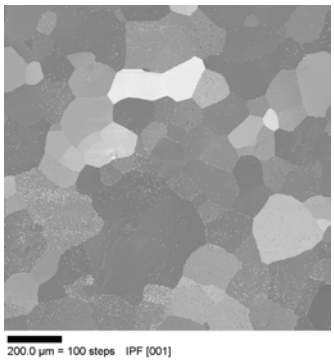

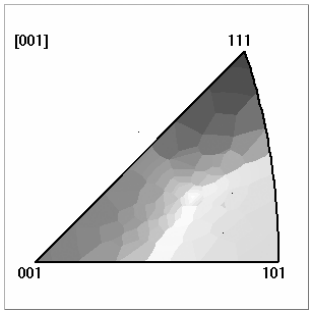

Fig. 1 - An inverse pole figure (IPF) map, also known as an orientation image map, of a 120 μm-thick Al foil annealed for 9 h at 550 °C, showing cube texture.

By contrast to the cube-textured Al foil, the boundary energy for the <111> fiber-textured, 1.7 μm-thick Al film showed significant variation in energy of high-angle boundaries (> 15° misorientation). In particular, there were two deep minima at misorientation angles of 28° and 38°. Interestingly, these misorientation angles are close to those for ∑13b boundaries at 27.8° and ∑7 boundaries at 38°. These results are in excellent agreement with the variation in grain boundary energy extracted from molecular dynamics simulations of grain boundary migration in aluminum by Upmanyu and others [19]. The common features include the general rise towards a peak around 35°, falling off towards 60°, along with the pronounced minima at the ∑13b and ∑7 positions. It is also worth noting that the strong <111> fiber means that the boundaries are all <111> tilts. Therefore the absence of a deep cusp at the ∑3 position is not surprising because, in this sample, these represent incoherent twins.

Table 1 gives the mean grain size and its standard deviation as a function of annealing time for the 100 nm-thick Al film. It is clear that grain growth stagnates after one hour of annealing, when the grains have nearly doubled in size from 68 nm to 134 nm. The grain size distributions given in Fig. 3 show that grain growth in the film is not self-similar, though the distributions for the different annealing times are not greatly different (Fig. 3). Examination of Fig. 3 for the population

of grains of a given size with annealing time up to the point of stagnation indicates an increase in the fraction of small grains. The grain size distribution for the 25 nm-thick film also shows a significant population of small grains relative to the mean grain size.

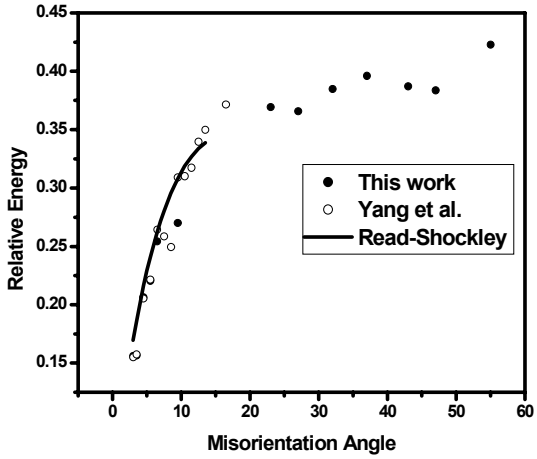

Fig. 2 - Relative grain boundary energy as a function of misorientation angle for the cube-textured Al foil.

Table 1 – Annealing time, mean grain size (equivalent circular diameter), standard deviation in grain size, and number of grains measured for 100 nm-thick Al films annealed at 400 °C.

Annealing time (h)	Average grain size (nm)	Standard deviation (nm)	Number of grains measured
0 (as-deposited)	68	29	1497
0.5	87	42	1304
1	134	73	1100
2	139	68	1353
4	146	75	1455
10	137	45	2022

Stagnation of grain growth has been previously attributed to the pinning of grain boundaries by grooves formed at the intersection of the boundary with the film surface.[20, 21] However, given the very stable oxide of Al formed upon exposure to air, grooves are not expected to form in this film. [22] Furthermore, grooving should pin the boundaries with low curvature, whereas the data of Fig. 3 indicates that it is the boundaries of small grains, which by necessity have high curvature, that are the affected boundaries. A similar argument would apply to solute drag as a source of boundary pinning, since again the low curvature boundaries should be the affected boundaries.[23]

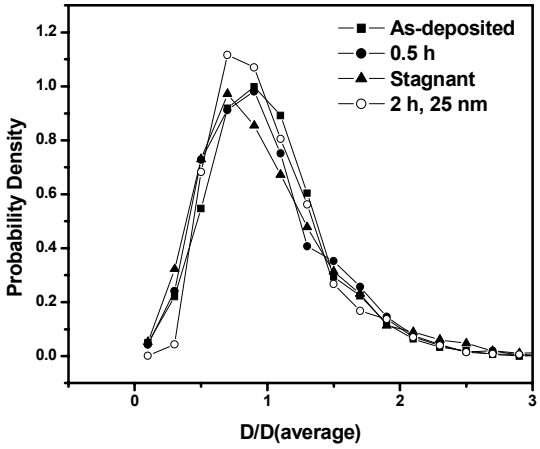

Fig. 3 - Probability densities for reduced equivalent circular diameter (size) of grains for annealed Al films. The open circles are the data for the 25 nm-thick film. All other data are for the 100 nm-thick films. The data for the stagnant structure is the combined data for samples annealed 1, 2, 4, and 10 h, given that grain growth stagnates after one hour of annealing as seen in Table 1.

In thin films, driving forces other than grain boundary energy reduction can promote grain growth. Examples include surface, elastic-strain and plastic-strain energies. The minimization of these energies favors the growth of certain subpopulation of grains and leads to the development of strong film texture.[24] However, for the films studied here, the minimization of these energies is not expected to play a significant role in either the initial grain growth or the eventual stagnation since the films were very strongly <111> fiber-textured even in the as-deposited condition and annealing resulted in minimal strengthening of this texture (Fig. 4). In addition, the Al films are in the zero stress, or low-compressive steady-state stress state at the annealing temperature and reach this state during heating to temperature.[25-27] Thus, film stress and its relaxation are also not expected to play a significant role in the observed grain growth and the subsequent stagnation.

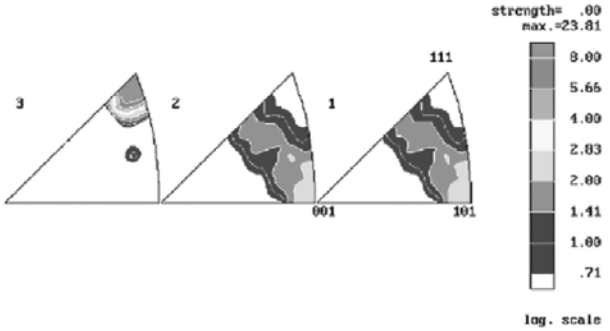

Fig. 4 – Inverse pole figures (IPFs) for the as-deposited 100 nm-thick Al film showing strong <111> fiber texture. (1) Rolling, (2) transverse, and (3) normal directions. In thin films with fiber texture, (1) and (2) are arbitrary directions. Examination of the IPFs for the 10 hour-annealed sample shows no significant change in the texture of the film compared with the as-deposited state.

For grain growth simulations, independent of the choice of simulation methodology (MC or PDE), and independent of the use of isotropic or anisotropic boundary energies, the distributions

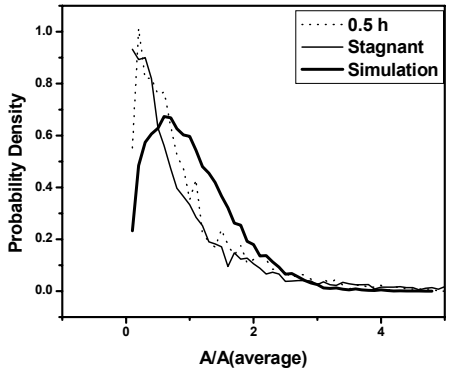

Fig. 5 – Comparison of reduced area probability densities for simulation and experiment (100 nm-thick Al films).

were in excellent agreement (not shown). There was no stagnation in growth and the distributions

were found to be self similar. Comparison of the simulated and experimental structures shows higher probabilities for small grains in the experimental samples, whether the grains are still growing (0.5 h) or whether they have reached the stagnant stage, as seen in Fig. 5. Thus, it can be concluded that grain growth in the 100 nm-thick Al films is neither well-represented by the 2D Monte Carlo model nor is by the 2D PDE model. The disagreement between experiment and simulation is either a consequence of the finite thickness of the films, given that thin films are not strictly 2D systems, or it implies the need for the inclusion of other terms in the equations for grain boundary motion. The impact of the finite thickness of the films was tested by examination of a thinner film (25 nm thick). As can be seen in Fig. 3, the 25 nm- and the 100 nm-thick films show little difference in the grain size distribution.

Conclusions

For the cube-oriented 120 μm-thick Al foil, the energies of low-angle boundaries increased with misorientation angle, in good agreement with the Read-Shockley model. For the high-angle boundaries there was little variation of energy with misorientation. In contrast, for the <111> fiber-textured, 1.7 μm-thick Al film, energies of high-angle boundaries showed significant variation with misorientation.

For the 100 nm-thick films, annealing at 400 °C resulted in the growth of grains until stagnation was reached at 1 h. Examination of the grain size distributions indicated that small grains were not disappearing as fast as they should. Comparison of the experimental distributions with the simulated distributions showed a significantly higher population of small grains in the experiments.

Support from the MRSEC program of the National Science Foundation under award number DMR-0079996 is gratefully acknowledged. P. Yu and I. Livshits are thanked.

References

1. S. Mahadevan, D. Casasent , Proc. SPIE Vol. 4735 (2002), p. 104.
2. C.C. Yang , W.W. Mullins, A.D. Rollett, Scripta Metall. Vol 44 (2001), p. 2735.
3. C. Herring: in the *The Physics of Powder Metallurgy,* ed. W. E. Kingston, (McGraw-Hill Book Co., New York 1951).
4. B. L. Adams, D. Kinderlehrer, W. W. Mullins, A. D. Rollett, and S. Ta'asan, Scripta Mater., Vol. 38 (1997), p. 531.
5. D. Kinderlehrer, I. Livshits, S. Ta'asan, and D. E. Mason, Proc. ICOTOM-12 (1999) p.1643.
6. B. L. Adams, D. Kinderlehrer, I. Livshits, S. Ta'asan, D. E. Mason, W. W. Mullins, G. S. Rohrer, A. D. Rollett, D. M. Saylor, and C.-T. Wu, Int. Sci. Vol. 7 (1999), p. 321.
7. D. Kinderlehrer, I. Livshits, D. Mason, S. Ta'asan, Interface Sci. Vol. 10 (2002), p. 232.
8. J. Kim, Ph.D. Thesis, Lehigh University, Bethelehem (2001).
9. http://www.scioncorp.com
10. K. Barmak, W. E. Archibald, A. D. Rollett, S. Ta'asan, D. Kinderlehrer, Mater. Res. Symp. Proc. Vol. 819, N6.6 (2004), p. 1.
11. D. Srolovitz, J. Vac. Sci. Technol. Vol. **A4** (1986), p. 2925.
12. D. Kinderlehrer, I. Livshits, S. Ta'asan, unpublished.
13. S. Ta'asan, P. Yu, I. Livshits, D. Kinderlehrer, J. Lee, Proc. 44thAIAA/ASME/ ASCE/AHS Structures, Structural Dynamics and Materials, Norfolk, VA, in press.
14. D. Kinderlehrer, I. Livshits, F. Manolache, A. D. Rollett, S. Ta'asan, Mater. Res. Soc. Symp. Proc. Vol. 652, Y1.5 (2001), p. 1.
15. W. T. Read and W. Shockley, Phys. Rev. Vol. 78, (1950), p. 275.
16. C. C. Yang. Ph.D. Thesis, Carnegie Mellon University, Pittsburgh (2000).
17. G. C. Hasson, C. Goux, Scripta Metall. Vol. 5 (1971), p. 889.
18. D. Wolf, J. Mater. Res. Vol. 5 (1990), p. 1708.

19. M. Upmanyu, D. Srolovitz, L. Shvindlerman, G. Gottstein, Acta Mater. Vol. 47 (1999), p. 3901.
20. W.W. Mullins: Acta Metall. Vol. 6 (1958), p. 414.
21. H. J. Frost, C. V. Thompson, D. T. Walton, Acta Metall. Mater. Vol. 38 (1990), p. 1455.
27. T. B. Read: *Free Energy of Formation of Binary Compounds – An Atlas of Charts for High-Temperature Chemical Calculations,* (The MIT Press, Cambridge, Massachusetts, 1971) p. 27. Equilibrium oxygen partial pressure for dissociation of aluminum oxide at 400 °C is 10^{-175} atm.
23. H. J. Frost, Y. Hayashi, C. V. Thompson, D. T. Walton, Mater. Res. Soc. Symp. Proc. Vol. 317 (1994), p. 431.
24. C. V. Thompson, R. Carel, Mater. Sci. Eng. Vol. B32 (1995), p. 211.
25. Gerth, D. Katzer, M. Krohn, Thin Solid Films Vol. 208 (1992), p. 67.
26. M. Legros, K. J. Hemker, A. Gouldstone, S. Suresh, R.-M. Keller-Flaig, E. Arzt, Acta Mater. Vol. 50 (2002), p. 3435.
27. J. Koike, S. Utsunomiya, Y. Shimoyama, K. Maryuama, H. Oikawa, J. Mater. Res. Vol. 13 (1998), p. 3256.